Probing the fate of interstitial water in bulk bioactive glass by ab-initio simulations

UNIVERSITÀ DEGLI STUDI DI TORINO

Probing the fate of interstitial water in bulk bioactive glass by ab-initio simulations

Enrico Berardo,[a] Marta Corno,[b] Alastair N. Cormack,[c] Piero Ugliengo[b] and Antonio Tilocca[*a]

[a] *Department of Chemistry, University College London, 20 Gordon Street, London WC1H 0AJ, United Kingdom; E-mail: a.tilocca@ucl.ac.uk*

[b] *Dipartimento di Chimica and NIS (Nanostructured Interfaces and Surfaces), Universitá di Torino, Via P. Giuria 7, 10125 Torino, Italy*

[c] *New York State College of Ceramics, Alfred University, Alfred, New York 14802, USA*

As also observed for conventional silicate glasses, water can be incorporated in the bulk interstitial regions of a bioactive glass (BG) matrix during the glass preparation and/or upon exposure to an aqueous environment. However, in the case of BGs, very little is known about the effect of hydration on the bulk structure, and then on key properties of these materials, such as biodegradation and bioactivity, that depend on the bulk structure itself. Here we employ a combination of atomistic simulation techniques to explore the nature and effects of water-BG interactions in the bulk of a bioactive glass. The fate of water inserted in the bulk interstitial region of 45S5 bioglass has been studied by ab-initio geometry relaxations and Molecular Dynamics (AIMD) simulations. We probed the interaction of a water molecule with silica rings and cages of different size, as well as the stability of potentially relevant configurations involving manually dissociated water and opened rings. The local stability of selected configurations was further assessed by subjecting them to AIMD runs, in order to overcome possible kinetic barriers for water diffusion and dissociation. Small rings do not appear as favourable absorption sites in the bulk of a bioactive glass as they are for bioinert glasses. Moreover, water dissociation through rupture of Si-O bonds of silica rings formed in the bulk resulted thermodynamically unfavourable. However, a high-temperature AIMD run led to a dissociated state involving no broken Si-O bonds and a free hydroxyl: because re-optimization of this state produced the most favourable hydration energy identified in this study, dissociative absorption through this mechanism appears a likely outcome of the water-45S5 interaction at low water content. We discuss the structural and dynamical basis for the stability of this and other water-glass adducts identified, and the potential consequences of these interactions for the behaviour of the glass in a biological context.

Introduction

Once in contact with the physiological environment of the human body, bioactive materials such as glasses and ceramics elicit a strong response in the surrounding medium, which leads to bonding to existing tissues (generally through a layer of bone-like calcium phosphates deposited on the materials' surface) and regeneration of new ones.[1, 2] Stimulated by the success in this context of the original melt-derived bioactive silicate glasses developed by Hench in the 1970s,[3] the field of bioactive glasses is in continuous expansion, with many other types of bioactive glasses having appeared in recent years or currently being explored, such as phosphate- and borate-based compositions,[4-6] as well as sol-gel glasses developed through low-temperature chemistry routes.[7] Different compositions or processing methods lead to glasses with variable dissolution rates and corresponding variable biological behaviour. For instance, the fast dissolution rates of borate and sol-gel silicate glasses lead to potential applications in the repair of soft tissues and as biodegradable scaffolds for tissue-engineering.[8-10] The very rapid biodegradation of phosphate glasses, on the other hand, limits their bone-bonding ability but promotes their use as antibacterial delivery vectors.[11] Another biomedical field critically affected by the glass biodegradation is in-situ radiotherapy, where a tumour is hit by radiation emitted by radioisotope ions carried and delivered within a biocompatible glass vector.[12] In this case, it is essential that the glass is stable with respect to dissolution and does not leach radioactive ions in the bloodstream during the treatment.[13]

The dissolution behaviour is clearly the key to tailor the performances of these biomaterials for the diverse applications highlighted above. The central role of the glass dissolution was further emphasized some years ago, when several studies highlighted an additional mode of bioactivity for conventional bioactive glasses, wherein critical amounts of soluble ions released by bioglasses such as 45S5 Bioglass® (BG45 hereafter) trigger the activation of osteogenic cells involved in tissue regeneration.[1, 14] It is now clear that understanding and controlling the dissolution of a bioactive glass is one of the main requirements for further progress in this field. Atomistic computer simulations represent one of the more powerful tools in this context, as shown by the large number of studies that have elucidated structural and dynamical features of bulk bioglasses and used them to clarify elusive links between composition, solubility and bioactivity.[15-20] Another highly relevant aspect that the simulations have started to address is the surface reactivity: in particular, ab-initio models have directly investigated the fundamental interactions between individual water molecules and the sites exposed at the bioglass surface,[21, 22] and also explored realistic interfaces between the glass and an aqueous contact medium.[23, 24] The information gathered through these studies now allows one to discuss and compare the potential surface reactivity of extended dry models of compact and nanosized bioglasses obtained by classical MD.[25, 26] This extends the current capability of the simulations to support a rational development of the biomaterials, complementing experimental probes such as Neutron and X-ray diffraction, Nuclear Magnetic Resonance and vibrational spectroscopy,[7, 16, 27-29] able to access structural details of the bulk glass and key features related to dynamical transformations following contact with physiological fluids.

Having elucidated the bulk structure of the dry glass and its surface interaction with water, a further step forward involves studying the interaction of water with the *bulk* region of the bioglass. Both high-temperature (melt and quench) or chemical (sol-gel) routes to prepare bioactive glasses lead to the incorporation and trapping of small amounts of water in the glass matrix.[30] This reflects the well-known incorporation of water in silicate glasses of mineralogical origin, as for instance for albite, rhyolite and basalt.[31-34] In these dense silicates water content is in the 0.06-6.9 wt. % range. Both infrared[31, 35] and NMR[36-38] spectroscopic studies revealed that water can sit inside the glass either molecularly or in a dissociated fashion giving rise to OH functionalities. The latter case dominates at very low water contents, with undissociated water becoming more important at higher water loading. Besides the small amounts of water "naturally" incorporated during the synthesis, water can be trapped in the bioactive glasses through another route: even though the initial contact with a biological aqueous fluid takes place at the external glass surface, water can penetrate within the glass matrix in the course of the surface dissolution and reconstruction processes involved in the bioactive mechanism.[2] This process will be facilitated by the fragmented structure of highly bioactive compositions such as BG45.[20]

Taking into account the well-known influence of water incorporation on physicochemical, optical and electrical properties of a glass,[39-42] presumably due to structural modifications introduced by the hydration process, these considerations highlight the importance of determining the fate of a water molecule absorbed in the bulk of a bioactive glass. For these biomaterials, it is especially important to assess whether and to what extent bulk absorption of water may affect the glass biodegradation, for instance by further disrupting – compared to the dry glass – the internal silicate backbone through rupture of Si-O-Si bonds, or through other mechanisms that involve interaction with and mobilization of modifier cations such as Na and Ca.[20] These effects are closely related to the molecular vs. dissociated state of absorbed water: because water dissociation in silica glass is typically associated with the breaking of Si-O bonds and formation of silanol (Si-OH) groups,[43] the latter process will result in the local trapping of water as relatively static Si-OH species. On the other hand, alternative dissociation pathways are in principle possible in modified silicate glasses, involving formation of free (i.e., not bonded to a Si) hydroxyl groups,[38] with a higher local mobility compared to silanol OHs.

Whereas – as mentioned above – some insight on the state of absorbed water has been obtained for conventional silicate and aluminosilicate glasses,[36, 44-46] no such information is available for bioactive glasses. In order to address this issue, in this work we examine in detail the behaviour of a water molecule set in contact with typical sites found in the bulk of BG45. It is important to remark that the bulk and surface structures of the glass, although obviously related, present some significant differences: strained or unstable interaction sites such as two-membered (2-m) rings and undercoordinated Si defects, formed on the as-created surface,[21] are absent in the bulk. Moreover, the silicate and phosphate speciation can also change on the surface compared to the bulk.[26] These effects presumably result in a host environment of different reactivity, and thus a different fate for a water molecule that reaches the bulk region, whose consequences must be understood. Another issue of interest concerns the mechanism and rate by which water can migrate within the bulk, a process that will also directly

affect the degradation and will ultimately depend on the nature of the glass-water interactions.

We have employed a combination of ab-initio structural optimizations and Molecular Dynamics runs to investigate the interaction of a water molecule incorporated within models of BG45 Bioglass®. The features of the most stable absorption sites identified and the observed reactivity (or lack thereof) are used to draw a description of the nature and mechanism of water incorporation and its potential effect on the biodegradation process.

Computational Methods

The calculations of this work were carried out on four independent BG45 samples of composition $32SiO_2$ $17Na_2O$ 19CaO $2P_2O_5$, hereafter named M1, M2, M3, M4, produced through a standard classical MD approach (see ESI for details).[47] The BG45 structures obtained by classical MD were then fully relaxed at the ab-initio (DFT) level with the CRYSTAL09 code,[48] using the B3LYP hybrid functional, an approach recently employed for the accurate determination of optimum geometries and phonon frequencies in bioglasses.[19, 22] The DFT-equilibrated bulk samples were then analysed for the presence of sites that could host an interstitial H_2O molecule, such as three-membered (3-m) and larger rings, and cages delimited by non-bridging oxygen atoms (NBOs). Once an H_2O molecule was inserted in a specific site, the interstitial H_2O/bioglass adduct was fully relaxed at the B3LYP level and the energy of the hydration process was computed together with its components, as defined below.

The stability of some representative H_2O/BG45 configurations obtained in this way was assessed by using them to start a new ab-initio (Car-Parrinello) MD run.[49] This method has been widely employed to model adsorption and reactivity of water at oxide and glass surfaces,[23, 50, 51] as well as dynamical processes within the BG45 bulk, such as ion migration.[52] CPMD trajectories of 10- 15 ps were run at 300 K to assess the stability of the optimized configuration. In each case, a ~ 60 ps CPMD run at 700 K was also carried out to accelerate the dynamics and explore a larger fraction of the configurational space, in some cases allowing the molecule to reach local minima that were not been initially located through the optimization. New stable configurations located in this way were then fully re-optimized with the CRYSTAL09 code, in order to calculate the corresponding hydration energies. Further specific details on the computational methods can be found in the supplementary information (ESI).

Hydration/Insertion Energy. The hydration energy, ΔE_H for a specific BG45 site, as defined below, corresponds to a negative value when the interaction between the molecule and the dry bioglass reference is stabilizing:

$$\Delta E_H = E(BW//BW) - [E(B//B) + E_M(W//W)] \quad (1)$$

where E(BW//BW) is the energy of a relaxed water/bioglass adduct, E(B//B) is the energy of the relaxed

bioglass dry reference and E_M(W//W) is the molecular energy of the free (gas phase) optimized H_2O molecule. The symbol following the // identifies the geometry at which the energy of the specific system is computed: for instance, E(W//BW) represents the (SCF) energy of an isolated water molecule frozen in the configuration corresponding to the optimized water-bioglass adduct. All calculations involve periodically repeated supercells, except those marked by the subscript *M* which denotes a molecular (nonperiodic) calculation.

ΔE_H can also be written separating the contributions of the deformation energy resulting from the change in geometry upon hydration of the BG45 dry reference (δE_B) and of the water molecule (δE_W), as follows:

$$\Delta E_H = \Delta E_H^* + \delta E_B + \delta E_W = \Delta E_H^* + \delta E_B + \Delta E_M + \Delta E_L \quad (2)$$

$$\delta E_B = E(B//BW) - E(B // B) \quad (3)$$

$$\delta E_W = E(W//BW) - E_M(W//W) \quad (4)$$

$$\Delta E_M = E_M(W//BW) - E_M(W//W) \quad (5)$$

$$\Delta E_L = E(W//BW) - E_M(W//BW) \quad (6)$$

$$\Delta E_H^* = E(BW//BW) - [E(B//BW) + E(W//BW)] \quad (7)$$

The deformation terms δE_B and δE_W are generally positive as they represent the difference between the energy of a fully optimized structure and the single-point energy of a non-optimized reference configuration frozen at the geometry adopted in the adduct. Equations 5 and 6 represent the two contributions that need to be considered when calculating the deformation of the water molecule: ΔE_M accounts for the inherent deformation of the molecule inserted in the bioglass, whereas ΔE_L takes into account the lateral interactions between the infinite water images in the configuration of the BW periodic adduct. The magnitude of ΔE_L is strongly dependent on the size of the periodic cell; the interaction of a molecule with its periodic image becomes almost negligible for larger cells (e.g. in our systems ΔE_L only contributes about 0.2 kJ/mol to the overall energy). ΔE_H^* is the hydration energy calculated with a reference in which both the dry bioglass and the water molecule, instead of being optimized as in Equation 1, are fixed to the final "deformed" configuration of the optimized BW adduct: ΔE_H^* can thus be considered a deformation- and lateral interactions-free hydration energy. Scheme S1 in the ESI provides a graphical representation of the various contributions.

Because our structural optimizations employ a localized Gaussian-type function basis set, ΔE_H needs to be corrected for the basis set superposition error (BSSE). The above ΔE_H definition can be recast to include the BSSE correction, using the widely accepted counter-poise method adopted for intermolecular complexes.[53] The definition of the final, BSSE-corrected hydration energy ΔE_H^C is then:

$$\Delta E_H^C = \Delta E_H^{C*} + \delta E_B + \delta E_W \quad (8)$$

$$\Delta E_H^{C*} = E(BW//BW) - [E(B[W]//BW) + E([B]W//BW)] \quad (9)$$

$$BSSE = \Delta E_H^C - \Delta E_H \quad (10)$$

where E(B[W]//BW) and E([B]W//BW) in equation (9) are the energy of the BG45 plus the ghost functions of the water molecule, and the energy of the infinite replicas of water molecules plus the ghost functions of BG45, respectively.

Results

In order to identify the most favourable absorption sites for the water/bioglass interaction, we discuss the trends in the hydration energies calculated for a series of sites located in the four different bioglass models. First, we focus on configurations generated through static geometry optimizations of the water/bioglass adducts, and then we investigate the effect of MD runs on selected water/bioglass configurations.

Dry models

Table 1 shows the properties of the B3LYP-optimized models of the four dry samples. The final density (*d*) of the optimized models is 5-7% higher than the experimental one, similar to the increase observed in DFT calculations of pure SiO_2 glass,[43] and slightly larger than the density of bulk BG45 models previously optimized with the PBE functional.[21]

The table also shows the number of small (three- to five-membered) rings present in each model. We probed the interaction of water with the 4-m and 5-m ring sites present in model 1, the 4-m ring in model 2 and the 3-m ring in model 3, shown in Fig. 1. The corresponding water-glass adducts will be hereafter labelled M1–r5, M1–r4, M2–r4 and M3–r3.

Table 1 Structure of the geometry-optimized BG45 samples and number of *n*-membered rings (*n* = 3, 4 and 5) in each model.

	Model			
	M1	M2	M3	M4
a (Å)	13.66	13.54	13.42	13.51
b (Å)	13.76	13.93	13.61	13.52
c (Å)	13.69	13.36	13.74	14.00
α (°)	90.77	91.00	89.54	89.57
β (°)	90.42	87.03	92.14	90.24
γ (°)	89.70	91.01	88.19	89.24
d (g/cm^3)	2.79	2.85	2.86	2.81
3-m rings	0	0	1	0
4-m rings	1	3	0	0
5-m rings	1	1	0	0

Furthermore, we probed three different open cages delimited by a high density of NBO species, found in model 1, model 2 and model 4, shown in Fig. 2 (the corresponding water adducts will be labelled M1–n, M2–n, M4–n, respectively). The cages are typically delimited by NBOs belonging to orthophosphate (Q^0) and Q^0-Q^2 silicate groups (a Q^n species is a Si or P atom bonded to *n* bridging oxygens), and also host several Na/Ca cations in their inner region.

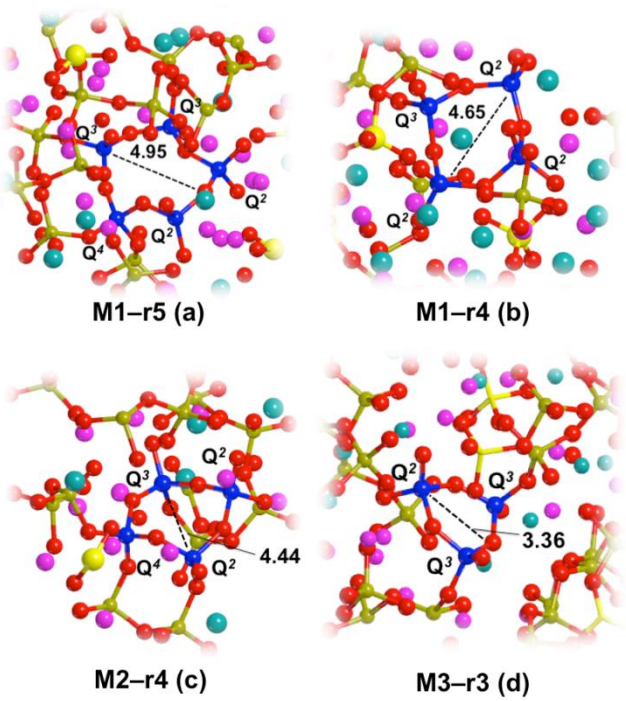

Fig. 1 BG45 rings probed in this work: (a) 5-m and (b) 4-m ring from model 1, (c) 4-m ring from model 2 and (d) 3-m ring from model 3. Colour codes are red (O), ochre (Si), yellow (P), magenta (Na) and cyan (Ca). The Q^n character of the Si atoms that constitute the rings is also shown, and these atoms are coloured in blue to differentiate them from the silicate network. The approximate size of each ring is shown in Å.

It is interesting to note that whenever we locate a cage large enough to accommodate a water molecule, orthophosphate groups and modifier cations are also found in its proximity. The mutual attraction between phosphate species and modifier cations (with a further preference for Ca-PO_4 over Na-PO_4 aggregation), as a consequence of the need to balance the negative charge of the orthophosphate,[54, 55] is well known and may play a decisive role for determining the final destination of a water molecule inside the glass matrix. Fig. 2 shows that in general the cages tend to be surrounded by silicate and phosphate groups with low or no connectivity, whilst by definition those species cannot be found in the rings, which are formed by Q^n species with $n \geq 2$.

Molecular water absorption

The structural constraints introduced by the BG45 matrix, with its high content of network modifying cations in close proximity to the above-mentioned rings and cages (Fig. 1 and Fig. 2), limit the number of possible starting configurations for water insertion at

each specific site. Particular care was then taken to ensure that all starting configurations did not contain unphysical short contacts such as Na(Ca)–H_w or O_W–NBO.

Water absorption at ring sites

M1–r5 The structural optimization of this adduct leads to a large rearrangement. The water molecule was initially placed inside the 5-m ring; during optimization it moved away from this inner region and formed a strong hydrogen bond (Hb) with a NBO from a Q^2 silicate group belonging to the ring (HO_W…H…NBO distances of 1.58 and 1.49 Å, respectively, almost a dissociated state). This final water/bioglass adduct (Fig. 3a) is characterized by an exothermic energy, (ΔE_H^C = -68.7 kJ/mol, Table 2). For this configuration, the large size and corresponding flexibility of the 5-m ring allow the water to reposition in a more stable arrangement (compared to the initial one where it was located right inside the ring) featuring favourable interactions with the NBOs of the silicate groups forming the ring.

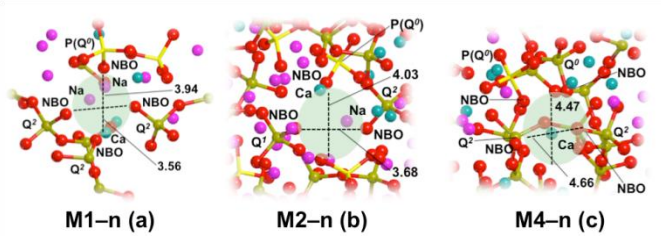

Fig. 2 BG45 cages studied in this work: (a) M1-n, (b) M2-n, and (c) M4-n. A light green shadow highlights the cage, and its approximated size (in Å) is also shown. Bold labels highlight the atoms (NBO, Ca, Na) lying inside or in proximity of the cage.

M1–r4 This structure rapidly converges to the final state (Fig. 3b), where the water molecule mainly interacts with NBOs from the 4-m ring. In particular, the molecule creates two hydrogen bonds with NBOs of silicate groups (Q^3 and Q^2) belonging to the 4-m ring, with the first interaction particularly strong (HOH…NBO distance of 1.46 Å). The spatial constraint exerted by the ring structure in this case appears stronger than in the previous (5-m) case and there is less freedom for the molecule to re-orientate and find more favourable interactions: this may explain the endothermic water insertion (ΔE_H^C = +119.4 kJ/mol). The number of modifier ions inside the water coordination sphere is exactly the same (three) as in the previous (exothermic) insertion, suggesting that the number of cations coordinated to water does not seem to affect the thermodynamics of the process in the case of absorption on rings, where the ring size and the corresponding spatial constraints seems to represent a more important factor.

M2–r4 Unlike the other ring insertion cases, in this optimized configuration (Fig. 3c) the water oxygen forms a direct bond (R(Si-O_w) = 1.86 Å) with a silicon atom of the ring, shown in blue in Fig. 3c, which then becomes penta-coordinated. Water also interacts with a Q^1 silicate and an orthophosphate (Q^0) nearby, but not contained in the 4-m ring; the HO-H…NBO distances of the first interaction (1.45 Å and 1.03 Å) indicate this case water can be considered dissociated by proton transfer to an NBO. This confirms the link between formation of water-silicon bonds and the probability of water dissociation, that has previously been highlighted for amorphous silica, see the Discussion section. However, Table 2 shows that the overall balance of these interactions still leads to an endothermic insertion (ΔE_H^C = 100 kJ/mol), mostly due to the high deformation contributions, that reflect a high energy cost needed to distort the two interacting subsystems in order to establish the new bonds and interactions described. This effect can be linked to previous indications[43] that the formation of Si-O_w bonds in silicate glasses requires significant structural distortions, in order to enable the molecule to closely approach a 4-coordinated silicon.

Table 2 Hydration/Insertion energy (ΔE_H^C) and its individual contributions (kJ/mol, Equations 1-10) for the absorption of a water molecule on different BG45 sites

Configuration	ΔE_H^C	ΔE_H	ΔE_H^*	ΔE_H^{*C}	δE_B	δE_w
M1–r5	-68.7	-145.4	-174.2	-97.5	18.6	10.2
M1–r4	119.4	33.2	-94.4	-8.2	114.0	13.6
M2–r4	100.4	19.6	-508.4	-427.5	301.8	226.1
M3–r3	119.8	41.0	-26.3	52.5	64.5	2.8
M1–n	-69.4	-156.6	-193.1	-105.9	25.4	11.1
M2–n	49.7	-22.0	-93.3	-21.7	67.2	4.2
M4–n	52.8	-39.9	-171.5	-78.8	114.5	17.1
M1–r5*	75.0	-23.6	-1339.7	-1241.2	533.2	783.0
M1–r4*a	132.6	36.4	-1400.1	-1303.9	732.8	703.7
M1–r4*b	-4.2	-78.4	-134.2	-60.0	50.5	5.3
M2–r4*	224.9	149.0	-1117.8	-1042.2	656.6	610.3
M3–r3*	134.8	45.3	-1250.7	-1161.2	493.2	802.8
M1–r4*b–MD	-91.3	-164.5	-185.2	-112.0	13.2	7.5
M2–n–MD	-53.1	-130.7	-255.5	-177.8	113.2	11.5
M2–n–MD–700	-155.1	-238.2	-193.1	-110.0	-51.1	6.0
M2–n*–MD–700	-169.9	-270.2	-1140.7	-1040.4	159.6	710.9
M4–n–MD	-16.3	-108.5	-261.1	-168.9	119.4	33.2

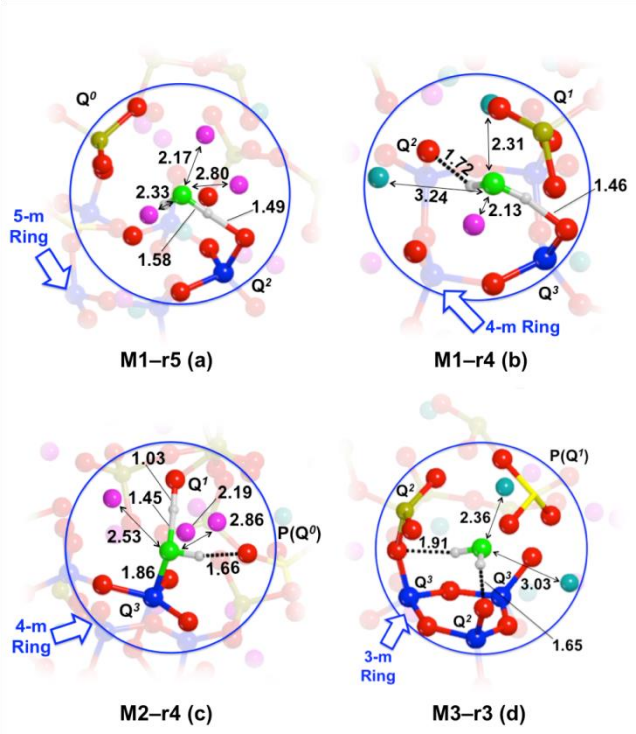

Fig. 3 Optimized water/BG45 configurations with water initially inserted in the proximity of a ring: (a) M1–r5, (b) M1–r4, (c) M2–r4 and (d) M3–r3. Colour codes are red (O), ochre (Si), yellow (P), magenta (Na), cyan (Ca). Si atoms forming the ring are blue and the water oxygen is green. Atoms contained inside the water coordination sphere (the sphere of radius 3.3 Å[23] centred on the water oxygen) are highlighted in the foreground, whereas the other atoms are shadowed. Hydrogen bonds are shown as bold-dashed dark lines. Relevant interatomic distances are shown. The arrows highlight the position of the relevant ring.

M3–r3 The water molecule initially located on the 3-m ring rapidly finds a stable configuration (Fig. 3d), where it still remains in direct contact with the 3-m ring through two relatively weak (HOH…O distances of 1.65 and 1.92 Å) Hb's, in particular with an NBO of a Q^2 silicate belonging to the 3-m ring, and a BO that connects the Q^3 silicate group of the 3-m ring and a Q^2 silicate outside the ring. The coordination sphere of the water oxygen in this case contains only two Ca ions. Table 2 shows that the insertion of a water molecule on a 3-m ring is an endothermic process (ΔE_H^C = +119.8 kJ/mol), mostly because the main water-BG interactions are weak: this is the only case where the deformation-free hydration energy ΔE_H^{*C} is also positive, showing that the underlying spatial constraints of the small ring do not allow the incoming molecule to create any favourable interactions with the substrate.

Water absorption at cage sites

M1–n After a substantial rearrangement, the molecule finds a stable minimum (Fig. 4a) characterized by an exothermic energy (-69.4 kJ/mol, Table 2) where it forms two Hbs with the NBOs of an orthophosphate (1.49

Å) and of a Q^2 silicate (1.74 Å). The central oxygen atom in this case has five modifier ions in its coordination sphere (four Na and a Ca).

M2–n This optimization leads again to a large structural rearrangement, where the displacement of the water molecule in the bulk is assisted by the concerted motion of the orthophosphate group facing the cage. The final configuration (Fig. 4b) features Hbs between water and the NBO of an orthophosphate (1.53 Å) and of a BO (1.58 Å) connecting two silicate groups (Q^1 and Q^2). The overall water insertion process in this case is endothermic (+49.7 kJ/mol), although still much more favourable compared to the strongly endothermic insertions at 3-m and 4-m ring sites, discussed above. Four Na ions populate the coordination sphere of water in the optimised structure.

M4–n In this optimisation the molecule creates two favourable Hbs with oxygen atoms from the Q^2 and Q^0 silicate groups, 1.45 and 1.82 Å long, respectively. Three modifier ions (two Na and one Ca) are within the water coordination sphere. As for the previous case, the water insertion for this configuration (Fig. 4c) is an endothermic process (+52.8 kJ/mol), but not as unfavourable as for the 3-m and 4-m ring insertions discussed before. Table 2 shows that the endothermic insertion processes in M2-n and M4-n cages reflect both higher deformation costs for the bioglass matrix and less favourable individual interactions (ΔE_H^{*C}), compared to the overall exothermic insertion in the M1-n cage. At variance from the ring absorption, the fact that the total number of modifier cations coordinating water is lower for the endothermic insertions denotes a possible effect of the site population of Na and Ca ions on the stability of the final adduct in the case of the cage sites, where the stronger constraint of the underlying ring structure is no longer present.

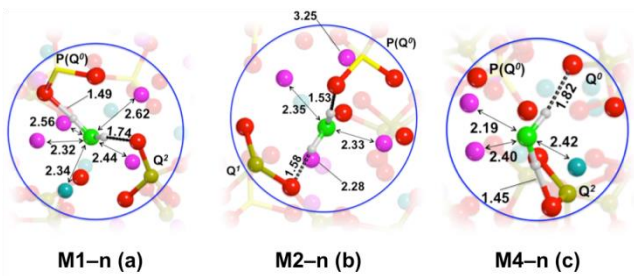

Fig. 4 Optimized water/bioglass configurations with water initially inserted in a BG45 cage. (a) M1–n, (b) M2–n and (c) M4–n. Symbols and notation are the same as in Fig. 3

Ring Hydrolysis

Si-O-Si bonds in strained silica rings exposed on silica surfaces are more prone to hydrolysis than those of siloxane chains not incorporated in small rings.[56] In the case of the amorphous SiO_2 surface, the thermodynamic driving force of the reaction is the release of the internal strain upon ring opening by water dissociation and formation of silanol groups, a process that may be hindered by an energy barrier.[51, 57] Water dissociation on small rings has been proposed to occur also in the bulk of amorphous silica.[43] It is thus worth investigating

further the possibility that water absorbed in the BG45 bulk may dissociate through the hydrolytic opening of this kind of ring. As the lack of spontaneous dissociation during the structural optimizations at ring sites discussed above may indeed reflect a high kinetic barrier, we evaluated the stability of the possible products by forcing the process, that is, manually breaking an Si-O-Si bond in 3-m, 4-m and 5-m rings, creating two Si-OH groups (as sketched in Fig. 5), and then relaxing the new configuration. Hereafter, a star appended to the label of BG45-water complexes denotes configurations where water was initially dissociated. The constraints imposed by the underlying structure, already mentioned before, limit the choice of ring ruptures: therefore for each ring we only investigated the hydrolytic rupture of a single Si-O-Si link, and considered different initial orientations of the silanols produced by dissociation.

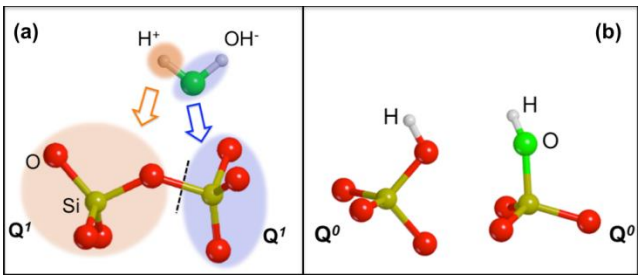

Fig. 5 Scheme of water dissociation at a siloxane bridge.

M1–r5*: Starting from the stable M1–r5 structure of Fig. 3a, the ring rupture by water dissociation was forced by transferring one of the water protons to a ring NBO(-Si) and attaching the remaining water OH^- to an adjacent Si of the ring. However, the Si-O-Si bridge was reformed during optimization, closing the 5-m ring again. The final configuration (Fig. 6a) thus contains a ring with a 5-coordinated Si, forming an Si-OH bond ($R_{Si\text{-}OH}$=1.95 Å) with the hydroxyl highlighted in green in Fig. 6a. The OH is coordinated by one Ca and four Na ions. The hydration process is endothermic by 75 kJ/mol, due the large deformation contributions that balance the favourable interactions established through the water dissociation.

M1–r4*a: Starting from the M1-r4 structure, a water proton was moved to saturate one of the NBOs from the 4-m ring, while the remaining OH^- was attached to an adjacent silicon also from the ring, breaking its Si-O-Si bond and opening the ring. The relaxed configuration (Fig. 6b) contains an Hb linking the Si-OH groups. Even though the 4-m ring does not reform in this case, the calculated hydration remains strongly endothermic, +132.6 kJ/mol, showing that the opening of the ring does not make the hydrolysis/dissociation process more favourable.

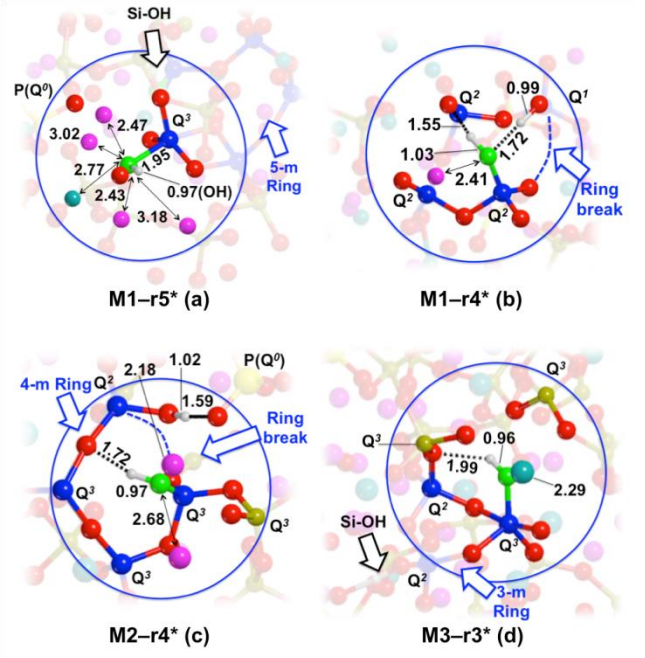

Fig. 6 Optimized water/BG45 configurations obtained after water dissociation at ring sites. (a) M1-r5*, (b) M1-r4*, (c) M2-r4* and (d) M3–r3*. Symbols and notations as in Fig. 3. The broken blue line shows the Si-O-Si link that was broken in order to hydrate the ring. When not visible in the foreground, the second Si-OH is highlighted by a black arrow.

M1–r4*b: In this alternative ring hydrolysis of M1-r4, achieved by a different initial orientation of the Si-OH groups, the 4-m ring is immediately reformed during the optimization and the initially dissociated water molecule also recovers its molecular state. In the final configuration (only shown in the ESI as it is essentially equivalent to the one discussed later in Fig. 7b), the reformed molecule is involved in two hydrogen bonds with NBOs from the ring. The hydration process in this case is almost thermoneutral, ΔE_H^C= -4.2 kJ/mol. This configuration seems to be a more stable counterpart of the M1–r4 configuration discussed before (Fig. 3b), as if a water molecule absorbed close to a ring may be able to reach a deeper local minimum only after an initial strong perturbation (such as that introduced by opening the 4-m ring), without which it tends to end up trapped in a shallower minimum.

M2–r4*: The 4-m ring remains open in the final configuration (Fig. 6c), while the silanols created by water dissociation are H-bonded with an orthophosphate's NBO and with a ring's BO. The silanol originated by the water's OH^- group has two Na cations in its coordination sphere. In this case the hydration energy is highly endothermic, ΔE_H^C = +224.9 kJ/mol, confirming the previous conclusion that the hydrolytic opening of a 4-m ring does not enhance the water absorption process.

M3–r3*: During optimization, the ruptured 3-m ring is reformed; thus the final configuration (Fig. 6d) contains a 5-coordinated Si with a Si-OH bond. Both silanols originated from the dissociation of the water molecule are involved in hydrogen bonds. The hydration energy in this case is again endothermic, ΔE_H^C =134.8 kJ/mol.

Effects of MD relaxation

A selected number of stable structures obtained through the static optimizations above was used to start Car-Parrinello Molecular Dynamics runs at 300 K and 700 K, with the purpose of confirming the (local) stability and eventually revealing other favourable minima not identified in the static approach. In the latter case, particularly stable configurations, as highlighted in the MD trajectories, were further re-optimized at the B3LYP level.

M1–r4*b–MD: During 10 ps of CPMD at 300 K the water molecule, initially H-bonded to two non-adjacent Si-NBOs of a 4-m ring, switches to two adjacent Si-NBOs on the same ring. This configuration then remains extremely stable (water does not further move or changes Hb partners) during 60 ps at 700 K. The structure re-optimized after the MD run is similar to the M1–r4*b discussed in the previous section, with the water molecule interacting with two NBOs of the 4-m ring through hydrogen bonds, and having one Na and one Ca cation coordinated to it; however, in this case the calculated hydration energy is exothermic by -91.3 kJ/mol. The high-temperature treatment thus leads to a more stable insertion structure, which may also reflect the fact that the whole glass structure has relaxed to a state intrinsically more stable than that yielded by the prior static calculation. In fact, Table 2 shows that, compared to M1–r4*b, the stability of the post-MD structure (M1–r4*b–MD) derives from a combination of more favourable glass-water interactions (ΔE_H^{*C}) and a lower glass deformation energy (δE_B).

M2–n–MD: During 14 ps of CPMD at 300 K, the water initially H-bonded to a PO_4 and a silicate BO (M2–n, Fig. 4b) gradually changes Hb partners to a different PO_4 and a Si-NBO (M2–n– MD, Fig. 7b, hydration energy -53.1 kJ/mol). During an additional 67 ps run at 700 K, the molecule hopped along different sites, eventually locating a particularly stable site featuring six modifier cations in its coordination sphere (M2–n–MD–700, Fig. 7c, ΔE_H^C = -155.1 kJ/mol). Subsequent spontaneous dissociation of this configuration then occurred by proton transfer to an NBO, whereas the remaining "free" hydroxyl moved away until locked in a cage of four Na and one Ca cations (Fig. 7d, -169.9 kJ/mol). This dissociated configuration, with the two OHs well separated, is the most stable one identified in this work, and, in fact, lasted unchanged for a relatively long time at 700 K, although in one instance, when the two OH's were able to approach each other again, they shortly recombined, reflecting the similar stability of the molecular and dissociated states just discussed.

M4–n–MD During 14 ps CPMD at 300 K started from the M4–n structure, the molecule that was initially H-bonded to two NBOs changed one NBO partner, but did not move significantly. Neither it moved during 65 ps at 700 K, even though at this temperature it occasionally switched Hb partner and in a few instances formed a short-lived pseudo-dissociated adduct. The corresponding re-optimized configuration shows that one of the Hb interactions involving an orthophosphate is indeed very strong (OH...NBO distance of 1.37 Å, M4–n–MD in Fig. 7e), recalling the pseudo-dissociated transient state just mentioned. Even though the underlying water-BG45 interactions have not changed, the post-MD structure is significantly more stable than the initial one, with an hydration energy of -16.3 kJ/mol (Table 2).

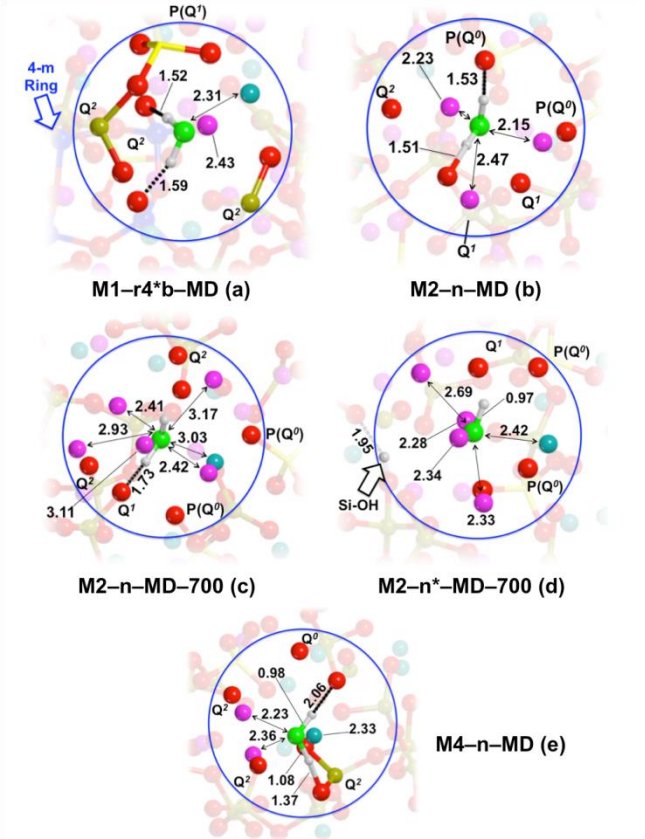

Fig. 7 Final configurations generated by optimizing structures sampled during CPMD trajectories. Symbols and notation as in Fig. 3.

Discussion

Ring sites control water absorption in amorphous SiO_2 (*a*-SiO_2). Pantelides et al.[45, 58] have shown that the most favourable absorption sites for *molecular* water in *a*-SiO_2 are large (7-membered or more) rings, where the molecule is easily accommodated in interstitial configurations with its protons H-bonded to bridging oxygens of the glass, and with an exothermic binding energy, on average. The stability of these configurations rapidly decreases with decreasing void size, with the insertion energy increasing by almost 200 kJ/mol in going from a 7 Å to a 4 Å void.[58] Additional, slightly less stable configurations involving a direct Si-O_w bond are also found in *a*-SiO_2; even though these configurations can in principle represent precursors for water dissociation, the corresponding dissociation energy is endothermic, suggesting that dissociation does not easily occur in unstrained (6-m or larger) *a*-SiO_2 cages, but most likely involves strained sites such as defects or smaller rings,[58] where the estimated reaction energies are in fact favourable.[45] Pantelides et al. then propose that water dissolved in *a*-SiO_2 is initially absorbed dissociatively close to small rings, and then, when no such rings remain available to dissociate water, additional water will be hosted in molecular state inside large rings. Similar conclusions were also reached by Van Ginhoven et al.[43], who also found that the most favourable absorption site in the water-*a*-SiO_2 system is a large cage, flexible enough to permit water to approach closely and form a covalent

bond to a Si: in fact, smaller cages do not allow H_2O-Si bonds to be formed. They also found that water dissociation is exothermic[43] only at sites close to strained three- and four-membered rings, becoming less favourable for the 4-m sites, and turning endothermic on larger rings. At variance with Pantelides et al., however, Van Ginhoven et al. question the possibility that water dissociation on *a*-SiO_2 requires the actual *rupture* of any small ring. They propose instead an indirect role of small rings, merely through the local creation of wider bond angles that enable close water approach and Si-O_w bonding in larger cavities, where dissociation can occur without ring rupture (i.e, the Si-O bond broken in the process does not belong to the small ring). In this case, the strain released would not be that of the ring itself, but that placed by the ring itself on its surroundings. In either case, it seems clear that dissociation of water absorbed in *a*-SiO_2 occurs at a distorted site, whose corresponding strain is released. This process can be seen as a dissociation-induced local annealing of the network, which prevents recombination of the silanols back to molecular water, and thus controls water retention in the glass by essentially trapping water in the form of silanols.[43] This also indicates that the stability of the water/glass adduct also reflects some water-induced relaxation of the glass network.

Our approach to probe sites such as rings and cavities of different size and shape in BG45, mainly based on the corresponding water binding energy after structure relaxation, is similar to that adopted to explore water absorption in *a*-SiO_2 in the studies above.[43, 45] Typical stable configurations found in *a*-SiO_2 involved water H-bonded to a silica bridging oxygen, weakly bound in a large void, or covalently bound to a Si atom,[43] with widely variable water insertion energies (ranging from -78 to +281 kJ/mol) that were ascribed to the broad length and angle distributions in the silica glass, as proven by the much narrower range measured for quartz. The BG45 substrate offers additional interaction sites for water, which are absent in *a*-SiO_2: namely, Na^+ and Ca^{2+} ions, and NBOs bonded to a range of different Q^n silicate and phosphate species. Previous experiments and simulations have shown that these sites can strongly bind water at the bioglass surface,[21, 59] and therefore can also be expected to introduce significant differences in the behaviour of a water molecule inserted in the bulk of these systems, compared to pure silica. As a matter of fact, the stable configurations identified in this study feature Na^+, Ca^{2+} or NBO in the water coordination sphere, with the cations coordinating the water oxygen as Lewis acids, and the NBOs behaving as strong hydrogen bond acceptors from the molecule. A few stable BG45/H_2O adducts also involve direct Si-O_w bonds. The most challenging issue, and the purpose of this work, was to rationalize how this complex network of interactions determines the fate of a water molecule once it reaches the bioglass inner regions. The break-up of the hydration energy in the individual contributions (ΔE_H^{*C}, δE_B, δE_w) provided additional information about their respective role on the stability of the hydrated adduct, and in particular on the effect of structural deformations introduced by the water-glass interaction. The values in Table 2 suggest that the overall stability of hydrated adducts is controlled by a subtle interplay of ionic and covalent interactions between the water molecule and the bioglass sites, and the deformations introduced by accommodating the molecule in each H_2O/BG45 geometry.

Small (3-m or 4-m) rings do not appear as favourable destinations for water absorption in BG45: the present results clearly show that molecular absorption is favourable on 5-m rings, but turns endothermic on smaller

rings. Therefore, it is unlikely that an interstitial water molecule will be attached to a small ring site in the BG45 bulk. Based on the results discussed above for *a*-SiO_2, we also considered the possibility that water may become trapped after dissociating at the ring sites. The results obtained for the initially dissociated configurations at rings seem to generally confirm the conclusion above: water dissociation/ring opening does not enhance the stability of water absorbed at small rings: the energies in Table 2 confirm that it is unlikely that water, either molecular or dissociated into silanols, will find a stable arrangement in the close proximity of a 3-m or 4-m ring, whereas it can – at least temporarily – be hosted in a stable molecular configuration close to a five-membered ring site.

The simulations also show that the rupture of a 3-m or 4-m ring does not represent a favourable mechanism for water dissociation and trapping in the bulk bioglass. The driving force of this process, for instance at surfaces, is often the internal strain released when a metastable ring is broken. Table 2 shows that for all configurations involving a ring rupture the deformation-free hydration energy (ΔE_H^{*C}) is in fact strongly exothermic, but it is counterbalanced by large deformation energies needed to perturb the glass structure (δE_B) and the water molecule (δE_W), distorting them to their final interacting geometries. The strain released by the hydrolytic ring opening thus does not appear sufficient to stabilize the corresponding water-BG45 adduct, and as a matter of fact in half of the cases examined here the original ring ruptured in the dissociation process is formed again.

Because the local strain present in the dry structure appeared to be the main factor driving water to interact strongly with small rings in *a*-SiO_2, the less favourable interaction observed between water and a 3-m or 4-m ring in BG45 can be linked to *reduced strain* associated to these sites. In fact, previous surface calculations had suggested that the fragmented nature of the BG network reduces the internal strain of exposed small rings, compared to pure silica.[20, 57] In the case of *a*-SiO_2, there can be a substantially higher energy gain resulting from the strain released either by rupturing a small ring (as proposed by Pantelides), or by hydrating a site associated to such rings (as proposed by Van Ginhoven). The different strain thus determines the different behaviour that we observe when water interacts with small rings in BG45.

The present simulations reveal how the large local distortion induced by ring hydrolysis can enable the molecule to locate a favourable minimum that would not be easily accessed otherwise: this may explain the outlier M1-r4*b case, for which Table 2 indicates that the deformation costs for reaching the final H_2O/BG45 adduct are much smaller compared to the ones required by its molecularly adsorbed counterpart (M1-r4). Whereas it is unclear whether the M1-r4*b can still be considered representative of water absorbed on a 4-m ring, this is an important indication that water-induced relaxations of the glass matrix can also contribute to determine the fate of the molecule in BG45, as will be further discussed below.

The silicate network connectivity (defined as the average number of bridging oxygens per Si^{60}) of BG45, around 2, is barely half that of *a*-SiO_2. One of the consequences is that the structure of BG45 is dominated by cross-linked chain fragments and the number of rings per unit volume is much lower than in pure silica. Moreover, even though a few large rings can still be found in BG45,[61] their inner region will always contain a large number

of modifier cations, so that they are deeply different from the large *empty* rings that, as summarized above, represent the most favourable water absorption sites in pure silica. In other words, no counterparts for the most stable water absorption sites of pure silica are available to absorb water in BG45. At the same time, the fragmented BG45 structure can give rise to relatively open NBO cages 4-5 Å wide, which may in some cases (such as M1-n) represent rather favourable absorption sites for molecular water, with exothermic hydration energy comparable to that of the 5-m ring. Rather than the cage size, the stability of the potential adduct where a water molecule is hosted in a cage seems to depend on the concentration of modifier cations hosted in the cage, as these cations are bound to interact with the molecule. Silica-free cages populated by network-modifier cations are related to the nano-segregated regions mainly populated with Ca^{2+} and PO_4^{3-} that form in higher-silica bioactive glasses.[20] As a matter of fact, phosphate groups are always found near the water molecule in the stable cage structures of Fig. 3. The hydration of these calcium phosphate cages is thus an important aspect, because it may affect the mobility and subsequent dissolution of calcium phosphate in the contact medium, a key step of the bioactive sequence.[62] Q^0 orthophosphate and orthosilicate groups appear to play an important role in stabilizing the water-cage adducts, as for the most exothermic M1-n configuration, but also the M4-n configuration, which despite the endothermic hydration energy, remains essentially unchanged even after a relatively long run at 700 K.

On the other hand, at finite temperature, the molecule absorbed in M2-n leaves the original cage and finds a different cage-like destination (Fig. 7c), where it is able to dissociate to a very stable state by transferring a proton to an NBO. Unlike the other dissociation cases considered before, in this case, the dissociation process does not involve any Si-O bond breaking, and results in the formation of a "free" hydroxyl group that rapidly separates from its original proton in the subsequent dynamics (M2-n* in Fig. 7d). This suggests that a necessary condition for the stability of the dissociated configuration in BG45 is the mobility of the "free" hydroxyl group created in the process. Taking into account the fact that the M2-n* configuration features the highest hydration energy identified in this work (Table 2), it may be proposed that Si-OH and free OH groups created *without* Si-O bond breaking may represent the most likely products of water dissociation in BG45, both because the energetic requirements for their formation is presumably lower as no covalent bonds need to be broken (δE_B for this case is in fact much lower than the ones observed for the ring rupture configurations), and also because the rapid departure of the free OH from the Si-OH left at the reaction site reduces the likelihood of a quick recombination to molecular water. Neither of these conditions are satisfied in the unsuccessful dissociation-induced ring openings examined. The stability of the free OH groups had already been highlighted at the BG45 surface,[21, 23] but also in the bulk of aluminosilicate glasses,[38, 46] and arises from the large availability (in these materials) of charge-balancing modifier cations able to cluster and form a protective cage around the OH groups.

Another key effect that emerged through the dynamics is the enhanced stability of the post-MD optimized structures, whose hydration energy is significantly more exothermic compared to the pre-MD one. In some

cases, such as M1-r4*b and M4-n, this occurs despite the main water-BG45 interactions being *apparently* unchanged during the dynamics. A possible explanation is that finite-temperature runs of several picoseconds enable a more complete long-range relaxation of the perturbation introduced in the BG by the incorporation of water, striking a favourable balance between the local reorganization of the BG atoms (especially of mobile species such as network modifying Na^+ and Ca^{2+}, and Q^0 groups) around the inserted molecule and the longer-range relaxation of the glass geometrical strain. A clear example of this trend is the case of the M2-n configuration produced by the CPMD run at 700 K, where the *negative* δE_B (-51.0 kJ/mol) implies that the dynamical run is able to relax the perturbed bioglass to such an extent that the energy of the BG depleted of the water molecule (E(B//BW)) is lower than that of the original dry reference (E(B//B)). The local water-cage interactions essentially trigger longer range relaxations of the whole glass network. These results also suggest that a dynamical approach may be a necessary supplement of static optimizations when phenomena involving bulk rearrangements of complex materials such as BG45 are investigated.

Conclusions

The energy landscape of a multicomponent invert glass such as BG45 results in a wide variety of metastable states for water absorption, which renders the investigation of water-glass interactions in this system a particularly challenging task. From a methodological point of view, this paper shows that a combination of static and dynamical calculations represents a suitable approach for adequately sampling the inner regions of the glass and for identifying the most relevant final states. The present calculations also show that the dissection of the hydration energy in its components, as proposed here, is useful to highlight the significant weight of the water-induced glass deformation on the overall thermodynamical balance of insertion, highlighting subtle long-range changes in the glass structures through the glass deformation energy term.

The bioreactivity of glasses such as BG45 in a physiological environment primarily arises from their very different structural features compared to conventional higher-silica compositions, such as high fragmentation and preferential association between modifier cations and less-connected silicate and phosphate fragments.[20] The present simulations show that these same structural features also determine a substantially different behaviour for a water molecule absorbed in the bulk glass. Whereas in amorphous silica water preferentially absorbs on small (3-m and 4-m) rings, where it dissociates forming silanol groups, rings of similar size do not appear as a favourable destination for a water molecule incorporated in BG45, neither in a molecular or dissociated state. For the reasons discussed above, the released strain associated to a small ring is not sufficient to enable water trapping by dissociation at these sites in BG45. Instead, stable molecular absorption states in BG45 involve larger (5-m) rings and silica-free cages hosting modifier cations able to coordinate water: the latter sites do not have equivalents in *a*-SiO_2, and are present in lower amounts in bioinert compositions. The strongest water-bioglass interactions for these favourable absorption modes involve hydrogen bonds between water and the NBOs of Q^n species with low *n*, such as orthophosphate groups, as well as coordinative bonds

between the water oxygen donor and the Na/Ca cations acceptors. Water absorbed in BG45 can then be temporarily trapped *in molecular state* in local energy minima associated to these cages. Albeit molecular water can survive for some time in these states, the evolution of one of the MD trajectories performed in this work also suggests that the molecule remains rather mobile, so that it can eventually escape to a new more stable cage that enables dissociation through proton transfer to an NBO and formation of a free hydroxyl stabilized by modifier cations and that can move away from the partner silanol. This overall dissociation mechanism does not involve Si-O bond breaking, and is thus fundamentally different from the mechanism effective in the NBO- and modifier-free *a*-SiO_2. It would be interesting to assess whether the same mechanism may be active in higher-silica bioinert glasses with a lower modifier content, especially in light of the experimental observation that OH diffusion is negligible in these materials.[34] In any case, the observed stability of the water molecule dissociated through this mechanism indicates that low amounts of interstitial water dissolved in BG45 will eventually be converted to silanols and free OH's.

An important question now concerns how the bulk incorporation of water through this mechanism may affect the glass biodegradation. As no Si-O bonds are broken in the process, the silicate network connectivity is not directly reduced by water absorption. Instead, a slight reduction in the number of charge-balancing NBOs can be expected when water dissociation occurs with the mechanism identified here, because free OH^- groups tend to attract modifier cations in their surroundings, removing them from the silicate network. In other words, one result of incorporation of small water amounts in the BG45 bulk may be a slight repolymerization of the glass network. Whereas this is in principle expected to lead to reduced biodegradation and bioactivity, at the same time the observed strong association between hydrous species and low-*n* silicate and phosphate Q^n species, as well as modifier cations, may enhance the dissolution of these soluble species, thus balancing the slightly higher connectivity of the silicate network. Further work will be needed to assess in detail how the overall balance between these individual effects is ultimately reflected in the way in which the glass matrix is degraded.

Finally, it is important to remark that the effects that we explored here are fundamentally distinct from those operating at the liquid-water/bioglass interface. In particular, here we focused on how low water contents dispersed within the bulk glass matrix, either during synthesis or upon penetration, can influence the stability of the matrix itself. The types and nature of glass interaction sites, as well as the aqueous phases involved, are very different from those characterizing the interface, and therefore the present results should not be considered directly representative of the glass *surface* degradation as described, for instance, by the Hench mechanism.[3]

Acknowledgments

A.T. gratefully acknowledges the UK's Royal Society for financial support. P.U. acknowledges Progetti di Ricerca di Ateneo-Compagnia di San Paolo-2011-Linea 1A, progetto ORTO11RRT5 for funding.

References

1. L. L. Hench and J. M. Polak, *Science*, 2002, **295**, 1014-1017.
2. J. R. Jones, *Acta Biomater.*, 2013, **9**, 4457-4486.
3. L. L. Hench, *Journal of the American Ceramic Society*, 1998, **81**, 1705-1728.
4. W. H. Huang, D. E. Day, K. Kittiratanapiboon and M. N. Rahaman, *J Mater Sci-Mater M*, 2006, **17**, 583-596.
5. M. Schuch, R. Christensen, C. Trott, P. Maass and S. W. Martin, *The Journal of Physical Chemistry C*, 2011, **116**, 1503-1511.
6. J. C. Knowles, *Journal of Materials Chemistry*, 2003, **13**, 2395-2401.
7. B. B. Yu, C. A. Turdean-Ionescu, R. A. Martin, R. J. Newport, J. V. Hanna, M. E. Smith and J. R. Jones, *Langmuir*, 2012, **28**, 17465-17476.
8. A. Yao, D. Wang, W. Huang, Q. Fu, M. N. Rahaman and D. E. Day, *Journal of the American Ceramic Society*, 2007, **90**, 303-306.
9. D. Arcos and M. Vallet-Regi, *Acta Biomater.*, 2010, **6**, 2874-2888.
10. R. A. Martin, S. Yue, J. V. Hanna, P. D. Lee, R. J. Newport, M. E. Smith and J. R. Jones, *Phil. Trans. R. Soc. A*, 2012, **370**, 1422-1443.
11. S. P. Valappil, D. Ready, E. A. A. Neel, D. M. Pickup, W. Chrzanowski, L. A. O'Dell, R. J. Newport, M. E. Smith, M. Wilson and J. C. Knowles, *Advanced Functional Materials*, 2008, **18**, 732-741.
12. E. M. Erbe and D. E. Day, *Journal of Biomedical Materials Research*, 1993, **27**, 1301-1308.
13. J. K. Christie and A. Tilocca, *Journal of Materials Chemistry*, 2012, **22**, 12023-12031.
14. I. D. Xynos, A. J. Edgar, L. D. K. Buttery, L. L. Hench and J. M. Polak, *J. Biomed. Mater. Res.*, 2001, **55**, 151-157.
15. Y. Xiang and J. Du, *Chem. Mater.*, 2011, **23**, 2703-2717.
16. C. Bonhomme, C. Gervais, N. Folliet, F. Pourpoint, C. C. Diogo, J. Lao, E. Jallot, J. Lacroix, J.-M. Nedelec, D. Iuga, J. V. Hanna, M. E. Smith, Y. Xiang, J. Du and D. Laurencin, *Journal of the American Chemical Society*, 2012, **134**, 12611-12628.
17. J. K. Christie and A. Tilocca, *J. Phys. Chem. B*, 2012, **116**, 12614-12620.
18. J. K. Christie, A. Pedone, M. C. Menziani and A. Tilocca, *J. Phys. Chem. B*, 2011, **115**, 2038-2045.
19. M. Corno, A. Pedone, R. Dovesi and P. Ugliengo, *Chemistry of Materials*, 2008, **20**, 5610-5621.
20. A. Tilocca, *Journal of Materials Chemistry*, 2010, **20**, 6848.
21. A. Tilocca and A. N. Cormack, *The Journal of Physical Chemistry C*, 2008, **112**, 11936-11945.
22. E. Berardo, A. Pedone, P. Ugliengo and M. Corno, *Langmuir*, 2013, **29**, 5749-5759.
23. A. Tilocca and A. N. Cormack, *ACS Applied Materials & Interfaces*, 2009, **1**, 1324-1333.
24. A. Tilocca and A. N. Cormack, *Proc. R. Soc. A*, 2011, **467**, 2102-2111.
25. A. Tilocca and A. N. Cormack, *Langmuir*, 2010, **26**, 545-551.
26. A. Tilocca, *Journal of Materials Chemistry*, 2011, **21**, 12660-12667.
27. R. A. Martin, H. L. Twyman, G. J. Rees, E. R. Barney, R. M. Moss, J. M. Smith, R. G. Hill, G. Cibin, T. Charpentier, M. E. Smith, J. V. Hanna and R. J. Newport, *Journal of Materials Chemistry*, 2012, **22**, 22212-22223.
28. M. Cerruti, D. Greenspan and K. Powers, *Biomaterials*, 2005, **26**, 1665-1674.

29. A. Goel, S. Kapoor, A. Tilocca, R. R. Rajagopal and J. M. F. Ferreira, *J Mater Chem B*, 2013, **1**, 3073-3082.
30. S. Lin, C. Ionescu, K. J. Pike, M. E. Smith and J. R. Jones, *J. Mater. Chem.*, 2009, **19**, 1276-1282.
31. E. Stolper, *Contrib Mineral Petr*, 1982, **81**, 1-17.
32. N. Zotov, Y. Yanev, M. Epelbaum and L. Konstantinov, *Journal of Non-Crystalline Solids*, 1992, **142**, 234-246.
33. S. C. Kohn, R. Dupree and M. E. Smith, *Geochim Cosmochim Ac*, 1989, **53**, 2925-2935.
34. Y. Zhang, E. M. Stolper and G. J. Wasserburg, *Geochim Cosmochim Ac*, 1991, **55**, 441-456.
35. K. M. Davis and M. Tomozawa, *Journal of Non-Crystalline Solids*, 1996, **201**, 177-198.
36. H. Eckert, J. P. Yesinowski, L. A. Silver and E. M. Stolper, *The Journal of Physical Chemistry*, 1988, **92**, 2055-2064.
37. T. Riemer, B. Schmidt, H. Behrens and R. Dupree, *Solid State Nuclear Magnetic Resonance*, 2000, **15**, 201-207.
38. Q. Zeng, H. Nekvasil and C. P. Grey, *The Journal of Physical Chemistry B*, 1999, **103**, 7406-7415.
39. D. B. Dingwell and B. O. Mysen, *Earth and Planetary Science Letters*, 1985, **74**, 266-274.
40. N. J. García, M. D. Ingram and J. C. Bazán, *Solid State Ionics*, 2002, **146**, 113-122.
41. S. Berger and M. Tomozawa, *Journal of Non-Crystalline Solids*, 2003, **324**, 256-263.
42. C. Cailleteau, F. Angeli, F. Devreux, S. Gin, J. Jestin, P. Jollivet and O. Spalla, *Nat Mater*, 2008, **7**, 978-983.
43. R. M. Van Ginhoven, H. Jonsson, B. Park and L. R. Corrales, *Journal of Physical Chemistry B*, 2005, **109**, 10936-10945.
44. N. Zotov, H. Keppler, A. C. Hannon and A. K. Soper, *Journal of Non-Crystalline Solids*, 1996, **202**, 153-163.
45. I. G. Batyrev, B. Tuttle, D. M. Fleetwood, R. D. Schrimpf, L. Tsetseris and S. T. Pantelides, *Physical Review Letters*, 2008, **100**, 105503.
46. J. Malik and A. Tilocca, *The Journal of Physical Chemistry B*, 2013, **117**, 14518-14528.
47. A. Tilocca, *Proc. R. Soc. A*, 2009, **465**, 1003-1027.
48. R. Orlando, M. Delle Piane, I. J. Bush, P. Ugliengo, M. Ferrabone and R. Dovesi, *Journal of Computational Chemistry*, 2012, **33**, 2276-2284.
49. R. Car and M. Parrinello, *Physical Review Letters*, 1985, **55**, 2471-2474.
50. Y. He, A. Tilocca, O. Dulub, A. Selloni and U. Diebold, *Nat Mater*, 2009, **8**, 585-589.
51. P. Masini and M. Bernasconi, *Journal of Physics: Condensed Matter*, 2002, **14**, 4133.
52. A. Tilocca, *The Journal of Chemical Physics*, 2010, **133**, 014701-014710.
53. S. F. Boys and F. Bernardi, *Molecular Physics*, 1970, **19**, 553-&.
54. M. W. G. Lockyer, D. Holland and R. Dupree, *J. Non-Cryst. Solids*, 1995, **188**, 207-219.
55. A. Tilocca and A. N. Cormack, *J. Phys. Chem. B*, 2007, **111**, 14256-14264.
56. B. C. Bunker, D. M. Haaland, T. A. Michalske and W. L. Smith, *Surface Science*, 1989, **222**, 95-118.
57. A. Rimola and P. Ugliengo, *The Journal of Chemical Physics*, 2008, **128**.
58. T. Bakos, S. N. Rashkeev and S. T. Pantelides, *Physical Review B*, 2004, **69**.
59. M. Cerruti and C. Morterra, *Langmuir*, 2004, **20**, 6382-6388.
60. Z. Strnad, *Biomaterials*, 1992, **13**, 317-321.
61. A. Tilocca, *The Journal of Chemical Physics*, 2013, **139**, 114501.
62. L. L. Hench, *J. Am. Ceram. Soc.*, 1991, **74**, 1487-1510.